RESEARCH ARTICLE

Characterization of key manufacturing uncertainties in next generation therapeutics and vaccines across scales

Miriam Sarkis[1,2] | Nilay Shah[1,2] | Maria M. Papathanasiou[1,2]

[1]Sargent Centre for Process System Engineering, Imperial College London, London, UK

[2]Department of Chemical Engineering, Imperial College London, London, UK

Correspondence
Maria M. Papathanasiou, Sargent Centre for Process System Engineering, Imperial College London, SW72AZ London, UK.
Email: maria.papathanasiou11@imperial.ac.uk

Abstract

Viral vectors are advanced therapy products used as genetic information carriers in vaccine and cell therapy development and manufacturing. Despite the first product receiving market authorization in 2012, viral vector manufacturing has still not reached the level of maturity of biologics and is still highly susceptible to process uncertainties, such as viral titers and chromatography yields. This was exacerbated by the COVID-19 pandemic when viral vector manufacturers were challenged to respond to the global demand in a timely manner. A key reason for this was the lack of a systematic framework and approach to support capacity planning under uncertainty. To address this, we present a methodology for: (i) identification of process cost and volume bottlenecks, (ii) quantification of process uncertainties and their impact on target key performance indicators, and (iii) quantitative analysis of scale-dependent uncertainties. We use global sensitivity analysis as the backbone to evaluate three industrially relevant vector platforms: adeno-associated, lentiviral, and adenoviral vectors. For the first time, we quantify how operating parameters can affect process performance and, critically, the trade-offs among them. Results indicate a strong, direct proportional correlation between volumetric scales and propagation of uncertainties, while we identify viral titer as the most critical scale-up bottleneck across the three platforms. The framework can de-risk investment decisions, primarily related to scale-up and provides a basis for proactive decision-making in manufacturing and distribution of advanced therapeutics.

KEYWORDS

advanced therapies, global sensitivity analysis, manufacturing, process flowsheeting, techno-economic analysis, uncertainty analysis, viral vectors

1 | INTRODUCTION

Advanced therapy medicinal products (ATMPs) are a new class of therapeutics that includes cell and gene therapies (C&GT), as well as tissue engineered medicines.[1] Their promising clinical results have made ATMPs particularly attractive for the cure of life-threatening diseases, including cancer and neurodegenerative disorders.[2] Currently,

there are approximately 700 on-going clinical trials for gene therapy products, while it is forecasted that by 2025 there will be 50–60 approved C&GT products in the market.[2–4] ATMPs are coupled with complex manufacturing processes that use advanced therapeutics as a "raw material." In that respect, viral vectors are the most frequently used carriers and find broad applications in ATMP manufacturing.[5–8] Owing to their ability to carry genetic payload, viral vectors have been established as one of the four most prominent vaccine manufacturing platforms.[9]

Despite prior knowledge, viral vector manufacturers faced significant challenges to ramp up capacity and respond to the unprecedented demand during the COVID-19 pandemic. As a result, the global viral vector manufacturing capacity was, almost exclusively, dedicated to COVID-19 vaccines, creating a backlog and possible shortages in the C&GT space.[4,10,11] This highlighted that, although clinically established, the viral vector industry is still immature when it comes to proactive and informed decision-making with respect to manufacturing capacity planning. The increasing demand and regulatory landscape pressures manufacturers to design cost-effective and reliable processes early on, guaranteeing global supply. This is not a straightforward exercise as product titers and product recoveries are reported to be low with respect to other biological products.[12] In this space, production planning activities become intrinsically *in risk*, as manufactures are faced with multiple decisions to make which are critically tied with uncertainties in process capabilities and future product demands.

Scale-up of cell-based, biological process is coupled with challenges related to the choice of suitable operating conditions that can ensure high product yield, cell growth and acceptable product quality.[10,11,13–21] To this end, viral vector manufacturers are focusing efforts to optimize their upstream (USP) and downstream (DSP) process train, integrating resilience to uncertainties arising from differences in physical and chemical environments. Such developments may result in higher yields and shorter production times.[12–15] Despite technological advancements in unit operation manufacturing and increased understanding of biological processes, process standardization, and intensification across scales remain a challenging task.[10,11,17] Building an understanding around the scalability and costs of manufacturing assets becomes increasingly important as underlying manufacturing uncertainties for processes under development may impact expected batch sizes, intrinsic process rates and costs. Such key performance indicators (KPIs) drive the decision-making and are critical for the long-term market success of any pharmaceutical product of this type.

In this space, computer-aided tools enable a systematic analysis of correlations between underlying manufacturing uncertainties and manufacturing KPIs. Recent efforts have been presented assessing process capabilities and performance under demand and process uncertainties in vaccines and ATMPs. Comisel et al.[22,23] developed a techno-economic model for LV and AAV manufacturing and assessed how inputs related to material costs and resource costs impact cost of goods sold (COGs) per dose, using local sensitivity analysis (LSA). Ferreira et al.[24] presented a bioprocess simulation in SuperPro Designer (Intelligen)[25] for AdV-based vaccine production to asses alternative USP process configurations, including batch versus perfusion mode of operation. The study proposed a what-if scenario approach to assess how USP titer impacts capital and operating expenditures comparing nominal process performance, at different scales. Kis et al.[26] developed SuperPro models for emerging vaccine platforms monitoring both the KPIs of interest and how those may impact supply chain decisions.[27] In a later study focusing on COVID-19 vaccines, Kis et al.[27] assessed the impact of manufacturing uncertainties during process development including batch failure rate, process scale, production titers, resource costs and their impact on process capital expenditure (CapEx), operating expenditure (OpEx) and throughput-related quantities. In this case, production scale is integrated as a continuous input, quantifying total production capacities and investments needed to deliver billions of COVID-19 vaccines and booster doses at global scale.[26]

Despite previous contributions in the field, the scale-dependent quantification of manufacturing uncertainty remains an open challenge. To address this, in this work we present a model-based framework to characterize process performance uncertainties, identifying which of those depend on process scale. Specifically, we assess how propagation of underlying manufacturing uncertainties affects investment and production planning performance indicators, such as batch size, process bottlenecks and costs. We aim to address the ongoing manufacturing challenges of *in risk* manufacturing for emerging pharmaceutical products. In the case where assets are fixed, maximizing process productivity is critical, as there may be limited flexibility to improve performance via capacity expansion. Investment in new capacity comes with added financial risks, which ought to be considered to quantify benefits of switching scale or scaling out production. In this context we quantify the impact of volumetric scale up and compare worst-case and best-case scenario performances at different scales. The former case is accounted for by sampling for lower viral titers, lower recoveries, and longer tasks, while the latter is quantified by sampling for improved titers, higher recoveries, and shorter process times. The proposed framework is applied to three industrially relevant viral vectors, currently at the forefront of advanced

manufacturing of biologics. A key novelty of the presented work is the use of computer-aided tools to quantify and compare scale-dependent process performance. This provides an important tool that can be used by technology developers and manufacturers to assess process feasibility and resilience early on. In the space of pharmaceuticals, the presented methodology can inform scale-up decisions from Phase I clinical trials to registration and authorization. The methodologies and approaches that form the backbone of this work are generic and can be tailored for any advanced manufacturing platform.

The remainder of the paper is organized as follows. Section 2 presents the modeling assumptions and data collected and structure of the techno-economic models and simulations and the global sensitivity analysis (GSA) workflow is explained. Results of the computational experiments are presented in Section 3, where cost-related and throughput-related uncertainties are compared for the three selected products and across scales. The significance of the results for investment planning and scheduling of viral vector supply chains is discussed, followed by a summary of key findings of the study in the concluding Section 4.

2 | METHODOLOGY

2.1 | Framework overview

The methodology developed in this study includes three main steps: (i) process flowsheeting, (ii) data collection, (iii) modeling and simulation, (iv) uncertainty and sensitivity analyses. Information regarding production processes for each of the viral vector manufacturing process are obtained from the scientific literature, for both drug substance (primary manufacturing) and drug product (secondary manufacturing). Each process flowsheet was created using SuperPro Designer.[25] SuperPro uses built-in sets of algebraic and differential equations to calculate material and energy balances, sizes equipment, schedules operations, and computes capital and operating expenditures. Information of techno-economic performance of the manufacturing platform can be obtained from each simulation. Variations in batch times that are related to process kinetics can be considered using our sampling approach. For the purposes of this study, we assume processes that have already been optimized and approved by regulatory authorities and therefore key process parameters, such as temperatures, pressures, medium, and buffer compositions are fixed.

In this study the outputs of interest are (i) batch size, (ii) batch time, (iii) cycle time, (iv) capital costs, (v) operating costs per batch, and (vi) unit production costs. Additional inputs are sourced from SuperPro's industrial-based databases. Operational inputs (e.g., task

lengths and recoveries, and working volumes) and resource costs are varied within the range reported in literature (known range) or an arbitrary range of ±50% of their nominal value (known nominal value, unknown range) in order to preserve the order of magnitude and allow assessment of input significance.

An uncertainty analysis (UA) is performed using a SobolGSA-MatLab-Component Object Model (COM)-SuperPro interface. The input samples are varied at each iteration and outputs of interest are recorded. This enables the generation of uncertainty distributions of the selected techno-economic outputs for each of the production processes. Global sensitivity analysis (GSA) is performed for every vector process to assess how vector-specific underlying manufacturing uncertainties propagate to KPIs differently according to the readiness of each production platform. By performing the UAs across scales, the variability of the KPIs is assessed by computing median and interquartile ranges (IQR). The latter indicates the range covered by the central 50% data points within the collected output samples. This allows a quantification of expected process batch sizes, process times and costs for each manufacturing scale to assess process scalability. The impact of the assumed input distributions on the output ranges is studied to illustrate scenarios where probabilities of input realizations may integrate knowledge gathered from process data. For this, uniform and triangular input distributions are considered and compared.

2.2 | Flowsheet development and data collection

Generalized processes for each of the vectors are modeled in SuperPro Designer. Detailed production recipes, resource costs are listed in Tables SI1-1–SI1-4. The following sections discuss key process steps, differences, and similarities across vector-products, namely adenovirus-based vaccines (AdV), lentivirus-based vectors for *ex vivo* gene therapy (LV), and adeno-associated virus-based *in vivo* gene therapies (AAV). Nominal values and ranges for process parameters and costs are listed in Tables SI1-5–SI1-8.

2.2.1 | Seed cell expansion

Adenoviral, lentiviral, and adeno-associated viral vectors

First, the working cell bank of HEK 293 cells is expanded in a series of cell culture steps (Steps 1–3, Figure 1A–C) upon addition of serum-free medium.[24,28] Each expansion step begins with a seeding cell density of 0.2×10^6 cells/mL. After 96 h of culture a cell density of 1.4×10^6 cells/
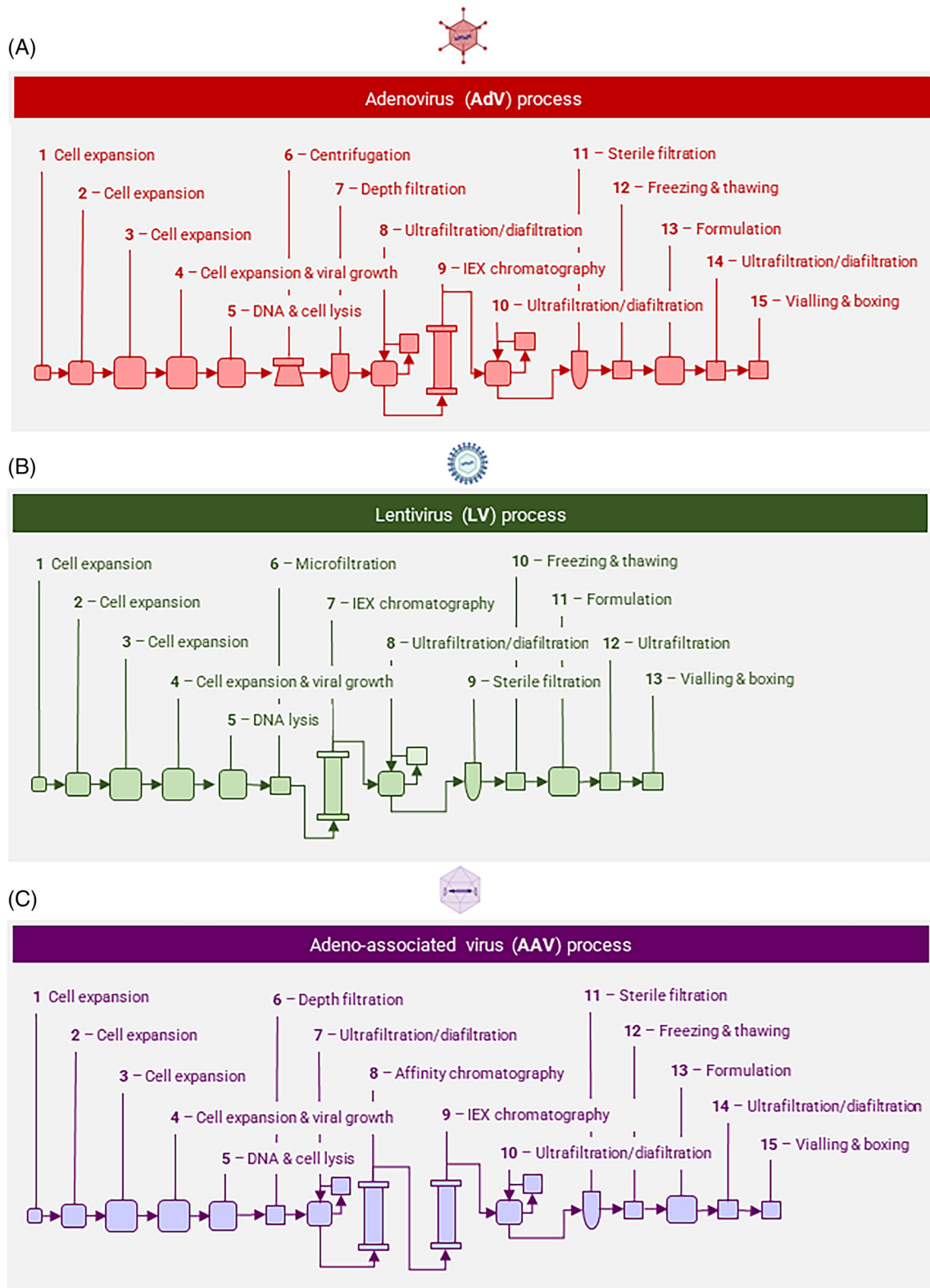
FIGURE 1 Flowsheet for: (A) Adenovirus manufacturing highlighting labeled process steps (1–15) and key resource inputs, (B) lentivirus manufacturing highlighting labeled process steps (1–13) and key resource inputs, and (C) adeno-associated virus manufacturing highlighting labeled process steps (1–15) and key resource inputs.

mL is reached and the culture is transferred to the subsequent step. The expansion factor for each step is 7, which results in 6 volumes of serum-free medium added at the beginning of each step.[29,30] Step 4 corresponds to the main bioreactor which operates at a working volume (WV) of 2000 L. Specifically, cells are expanded for 3.6 days to a cell

density of 1.9×10^6 cells/mL. At each step the culture is aerated via a mixture of air and CO_2, with the latter added to maintain pH during cell growth.

2.2.2 | Viral growth

Adenoviral, lentiviral, and adeno-associated viral vectors

Viral growth is the initiated via two routes in Step 4. (Figure 1A–C). In the case of AdV, infection-based viral growth is assumed, which entails the cell culture being infected via the addition of concentrated AdV master virus bank at 1×10^{12} VP/mL.[24] In the LV and AAV processes, transfection-based viral growth is assumed, with 2.5 μg/10^6 cells of plasmid DNA added to the culture.[22,23] Both the transfection and infection step take 48 h and progress until a target titer is reached, namely 1×10^{11} VP/mL (AdV),[13,20,21] 1×10^7 TU/mL[20–22,31–33] (LV), and 1×10^{11} vg/mL (AAV).[23,34–36] The culture is then harvested and the mixture is clarified. As viral vectors are either intracellular (AdV, AAV) or extracellular (LV) products, vector-specific DSP are modeled accordingly.

2.2.3 | Primary recovery

Adenoviral and adeno-associated viral vectors

AdV and AAV vectors are intracellular products and require breakage of HEK cells to be released in the supernatant. Cell lysis (Step 5, Figure 1A,C) is performed by adding 1 mL/10^7 cells of lysing agent Triton X-100.[20] The mixture is incubated, and complete cell lysis is assumed. After cell lysis, DNA is then degraded via a DNA lysis step with the addition of 25×10^6 U/mL of feed of Benzonase,[22,23] for AAV and AdV. In the AdV process, the mixture is centrifuged (Step 6, Figure 1A) to remove cell debris, precipitated nucleic acids and cell debris. A depth filtration step (0.2 μm membrane) (Step 7, Figure 1A) removes the remaining particulate components in the stream. The mixture is sent to a ultrafiltration/diafiltration (UF/DF) (0.005 μm membrane) (Step 8) system with impurities removed via the permeate and AdV viral particles retained by the membrane. In the AAV process, a microfiltration step (0.45 μm) (Step 6, Figure 1C) removes cell debris, precipitated nucleic acids and impurities after lysis and substitutes the AdV centrifugation and depth-filtration step. The AAV mixture is sent to a UF/DF system (Step 7, Figure 1C) with impurities removed via the permeate and AAV viral particles retained by the UF membrane.

Lentiviral vectors

As LV vectors are extracellular products cell lysis is not required. DNA degradation is achieved by adding the same amount of Benzonase (25×10^6 U/mL feed) (Step 5, Figure 1B). Viral losses in this step are ignored as negligible[24,37] with respect to the more significant losses in the following steps. A microfiltration step (Step 6, Figure 1B) removes cells and precipitated nucleic acids. The clarified LV mixture is sent to a chromatography step.[22,23]

2.2.4 | Purification

Adenoviral vectors

The AdV retentate from the UF/DF step is sent to an ion-exchange (IEX) chromatography column (Step 9, Figure 1A), which removes protein and DNA impurities. The retentate is loaded onto the column with a binding capacity of 3×10^{12} VP/mL[19,24] and a binding efficiency of 100%. The column is washed to remove weak impurities. Elution of AdV product is achieved with the gradient addition of a NaCl-based buffer to shift pH of the column. An overall AdV yield of 80%[24,38] is assumed. The column is then regenerated with a high-concentrated NaCl-based buffer (>20/gL) to desorb strong impurities. Finally, re-equilibration is achieved by wash buffer, marking the start of a new cycle.

Lentiviral vectors

The same purification protocol (Step 7, Figure 1B) is implemented in the LV process, with adjusted recoveries and binding capacity. The retentate is loaded onto the column with a binding capacity of 5×10^8 TU/mL[18,22,23] and a binding efficiency of 100% and overall step recovery of 40%.[18,22,23]

Adeno-associated viral vectors

In AAV purification, an affinity chromatography column (Step 8, Figure 1C) precedes the IEX step[23] (Step 9, Figure 1C), as it is reported that IEX alone cannot separate full capsids from empty ones.[39–41] A neutralization tank is added after affinity chromatography is performed. The two columns are modeled with a binding capacity of 3×10^{12} vg/mL and 1×10^{13} vg/mL respectively,[23,42] with yields of each step assumed to be 70%.[23] The cycles follow those of the AdV process. The viral titer after IEX is specified in the model as 1.12×10^{12} vg/mL.[23,42]

2.2.5 | Polishing

Adenoviral vectors

Polishing of the viral vector solutions is achieved with UF/DF and sterile filtration. AdV is concentrated by a

factor of 3 (Step 10, Figure 1A). The mixture is diafiltered with seven volumes of formulation buffer, as vectors are unstable after IEX. The solution is then flushed with a volume of 20 L/m^2 and average permeate flux of 30 L/m^{2}h resulting in a viral particle concentration of 2.1×10^{12} VP/mL.[24] The overall viral yield of the process step is set to 90%. The formulated bulk is sterile-filtered (0.2 µm membrane) with a flux of 2000 L/m^{2}h and an assumed loss of 5% and a titer 2×10^{12} VP/mL (Step 11, Figure 1A). The drug substance bulk is frozen and stored at $-70°C$ using liquid N$_2$ for heat exchange (Step 12, Figure 1A).

Lentiviral vectors

The LV purified solution is ultrafiltered/diafiltered (Step 8, Figure 1B) for buffer exchange and this is prototyped on the AdV process. The adjusted product recovery for this step is 80%, with a final drug substance titer of 9.8×10^8 TU/mL, which falls in the range of 10^8–10^9 TU/mL.[22] The drug substance is sterile-filtered (0.2 µm membrane) (Step 9, Figure 1B) and cryofrozen to $-70°C$ with liquid N$_2$ and stored (Step 10, Figure 1B).

Adeno-associated viral vectors

The AAV purified solution is ultrafiltered/diafiltered (Step 10, Figure 1C) for buffer exchange and this is again prototyped on the AdV process. The adjusted product recovery for this step is 95%, with a final drug substance titer of 2.3×10^{12} vg/mL.[23] The drug substance is sterile-filtered (Step 11, Figure 3), and cryofrozen to $-70°C$ with liquid nitrogen and stored (Step 12, Figure 1C).

2.2.6 | Fill and finish

Adenoviral vectors

The AdV drug substance is thawed and formulated with PBS buffer to a target concentration of 10^{11} VP/mL[43,44] (Step 13, Figure 1A). The solution is sent to UF step and filled into 5 mL vials[43,44] at a rate of 400 vials/min[45] and 3 parallel lines (Step 14, Figure 1A). This allows each vial to contain 10 doses.[43,44] Each vial is capped, labeled, refrigerated at 2°C[43,44] and boxed (Step 15, Figure 1A).

Lentiviral vectors

The LV drug substance is thawed and formulated with PBS buffer and concentrated/ultrafiltered to a target concentration of 2×10^9 TU/mL in 50 mL vials (Step 11-12, Figure 1B).[7,23] Vials are filled at a rate of 10 vials/min[45] which are then capped, labeled, cryofrozen, and boxed (Step 13, Figure 1B).

Adeno-associated viral vectors

The AAV substance is thawed and formulated with PBS buffer and concentrated/ultrafiltered to a target concentration of 1×10^{13} vg/mL in 50 mL vials[5,6,23] (Step 13-14, Figure 1C). Vials are filled at a rate of 10 vials/min[45] and are then capped, labeled, cryofrozen, and boxed (Step 15, Figure 1C).

2.2.7 | Outputs

The monitored model outputs can be divided in throughput- and cost- related outputs (Figure 2A). The *batch size B* of each process is calculated based on the mass flow per batch. The assumed dose sizes relate to the 3 selected representative product applications, namely vaccines as 5×10^{10} AdV viral particles (VP)/dose,[43,44] *in vivo* gene therapy as 7×10^{14} AAV viral genomes (vg)/dose,[5] *ex vivo* gene therapy as 2×10^9 LV transfecting units (TU)/dose.[7,22,23] The *batch time T* is calculated as the time to process the batch from USP to fill and finish (F&F). The *cycle time Y* is defined as the minimum required time before another batch can be started (i.e. bottleneck step).

The *capital cost* includes direct fixed capital (DFC) costs C_1, start-up and validation C_2 and working capital costs C_3. DFC includes equipment purchase cost and estimates costs of installation, piping, and building. Start-up and validation cost is calculated as a percentage of DFC.[25] Working capital is instead defined as the upfront expenditure required to cover the first 30 days of operation in terms of variable costs. It therefore depends on the variable-related OpEx per batch (materials O_1, consumables O_4, utilities O_5) and how many batches can be completed within the starting 30 days.

The *operating cost* includes raw material costs (medium, buffers, lysing agents, plasmid DNA, and HEK cells), consumables (chromatography resins, filter membranes), utilities, labor costs, QC/QA costs and facility dependent costs. The variable costs (materials O_1, consumables O_4, utilities O_5) are calculated based on resource costs reported in literature (Table SI-8) and SuperPro industrial-based materials database. The labor costs O_2 are calculated based on an assumed basic labor rate 30 \$ h^{-1}[25] and on the calculated batch time T.

The assignment of labor to each process step can be specified by an allocation factor, which relates the number of labor hours to the actual process time. A value >1 would indicate that operators would work in parallel on a specified task. In this work, a value of 1 is assumed for all units. The quantified labor hours are multiplied by lumped labor rate, which is calculated based on the input basic rate and accounting for benefits, supervision, supplies and administration requirements.[25,46] The underlying correlations are
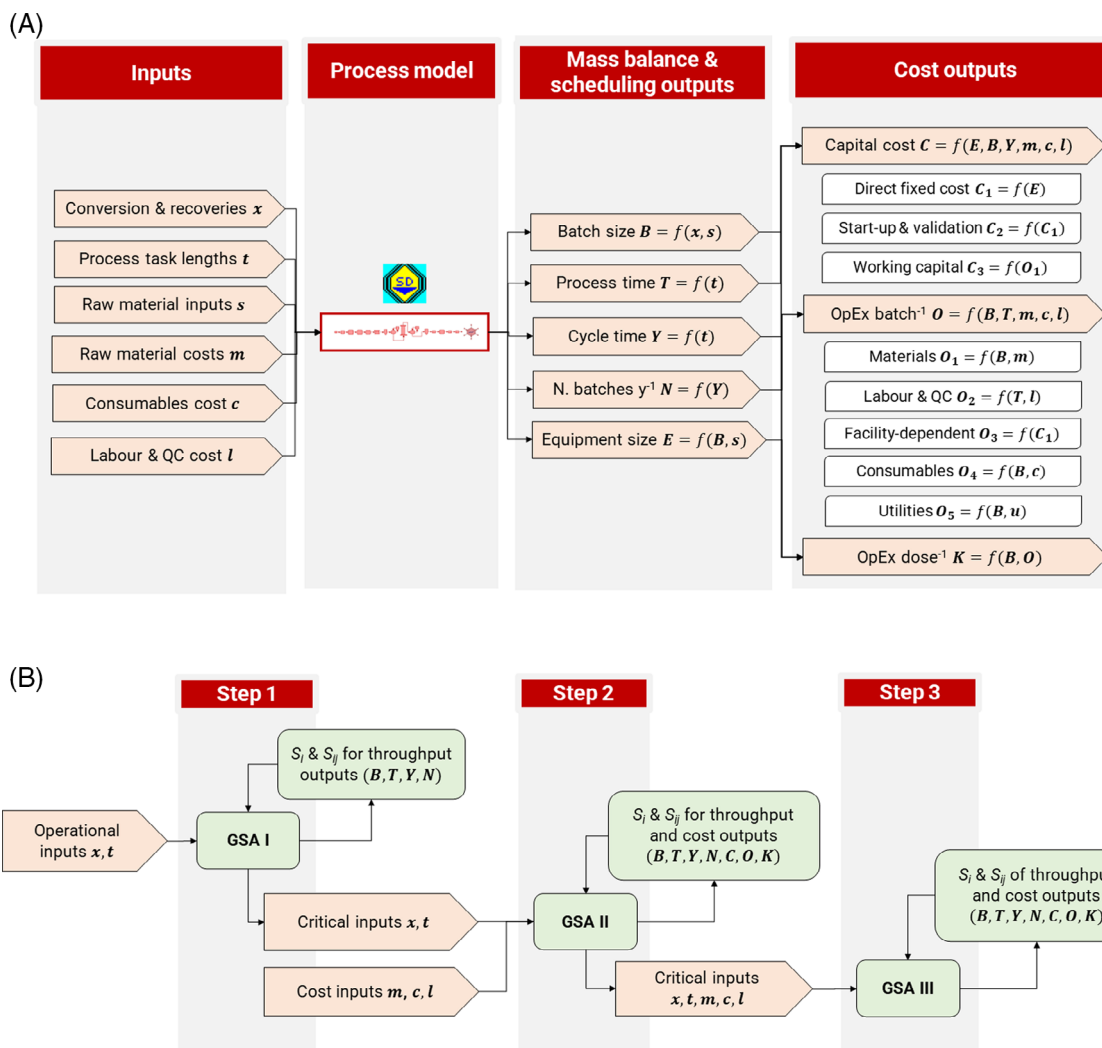
(A)

Figure content with Inputs, Process model, Mass balance & scheduling outputs, and Cost outputs:

Inputs
- Conversion & recoveries x
- Process task lengths t
- Raw material inputs s
- Raw material costs m
- Consumables cost c
- Labour & QC cost l

Process model

Mass balance & scheduling outputs
- Batch size $B = f(x, s)$
- Process time $T = f(t)$
- Cycle time $Y = f(t)$
- N. batches y^{-1} $N = f(Y)$
- Equipment size $E = f(B, s)$

Cost outputs
- Capital cost $C = f(E, B, Y, m, c, l)$
  - Direct fixed cost $C_1 = f(E)$
  - Start-up & validation $C_2 = f(C_1)$
  - Working capital $C_3 = f(O_1)$
- OpEx batch^{-1} $O = f(B, T, m, c, l)$
  - Materials $O_1 = f(B, m)$
  - Labour & QC $O_2 = f(T, l)$
  - Facility-dependent $O_3 = f(C_1)$
  - Consumables $O_4 = f(B, c)$
  - Utilities $O_5 = f(B, u)$
- OpEx dose^{-1} $K = f(B, O)$

(B)

Step 1
- Operational inputs x, t → GSA I
- S_i & S_{ij} for throughput outputs (B, T, Y, N)
- Critical inputs x, t
- Cost inputs m, c, l

Step 2
- GSA II
- S_i & S_{ij} for throughput and cost outputs (B, T, Y, N, C, O, K)
- Critical inputs x, t, m, c, l

Step 3
- GSA III
- S_i & S_{ij} of throughput and cost outputs (B, T, Y, N, C, O, K)

FIGURE 2 (A) Overview of layers of calculations embedded in techno-economic model and (B) Three-step global sensitivity analysis (GSA) workflow. Step 1: highest-ranking $(S_i + S_{ij} \geq 0.05)$ operational inputs are obtained, which impact batch size B, T, Y, N throughput-related outputs. Step 2: the screen operational inputs are combined with resource costs inputs. GSA determines the highest-ranking inputs within the operational and resource costs input space. Outputs monitored in GSA II include capital costs and operating costs C, O, K. Finally, GSA III is performed to obtain results displayed in Section 3.3. All plots for Step 1–3 are included in SI.2.

included in Section SI1-7. QC/QA costs are calculated as a percentage of this.[14] Finally, facility dependent costs O_3 are calculated as a percentage of DFC and account for the contribution of maintenance and equipment depreciation to the operating costs. In this study, OpEx per batch and OpEx per dose are selected as outputs.

Different scales of productions are considered for each vector product, namely 50, 200, 1000, and 2000 L scale (main bioreactor working volume). The throughput of the facility is adjusted via a user-defined factor which scales flows in each material balance calculation. Process models are simulated for the selected scales and products, thereby solving material balance, equipment sizing and costing equations. The techno-economic performance of each process plant at this nominal value is recorded and the cost breakdown is analyzed.

The outputs selected offer an overview of an overall process throughput, time, capital, and operating costs. The output set can however be augmented to section-specific quantities and/or individual cost components depending on the detail of the analysis required. This may find an application techno-economic assessments of multi-purpose production platforms.

2.3 | Global sensitivity analysis and uncertainty analysis

The impact of parameter and process uncertainties on the model outputs can be quantified by sensitivity and uncertainty analyses. To align with current industrial practices, where campaign planning and process

8 of 20 | WILEY
JOURNAL OF
ADVANCED
MANUFACTURING
AND PROCESSING

SARKIS ET AL.

improvements take place post the establishment of the process units, equipment size is fixed for all process models. In such cases, the productivity of the process may decrease due to limited understanding of the volumetric scale up or improve with process engineering and optimization. This enables characterization of a *productivity space* for each manufacturing scale. Given a set of inputs, the framework samples from the associated probability distributions of each input and records all calculated outputs. Operational inputs (e.g., task lengths, conversions, and recoveries) and resource costs are considered and their impact on the selected KPIs (Section 2.2) is monitored.

2.3.1 | Global sensitivity analysis

The input–output sensitivities for each flowsheet are assessed using Sobol sequence. For this the techno-economic model is simulated iteratively for 4096 quasi-random input samples. Variance-based global sensitivity analysis (GSA) is performed to investigate the respective contributions of input uncertainty to the recorded outputs. Given the dimensionality of the input–output model, random sampling-high dimensional model representation (RS-HDMR) is implemented. The method relies on the generation of a metamodel from input–output data and requires the additional samples (1023) to simulate the process and the test the validity of the surrogate. All inputs are varied simultaneously, and the output variance is recorded. This allows the computation of indices which inform on both single input contributions to output variability (first-order indices, S_i), combined contributions of inputs i and j (second-order indices, S_{ij}), as well as higher order interactions. The total contribution of a single input (S_T) is also calculated, by summing up first, second and higher orders interactions. Here we assume first-, and second-order interactions and calculate: $S_T = S_i + S_{ij}$. Higher order interactions are excluded as insignificant.

Given the computational complexity of considering all operational inputs and resource inputs (Tables SI5–8), a three-step GSA-based methodology is proposed to screen inputs and preserve key sensitivities of the outputs (Figure 2B). The methodology takes advantage of the layers of calculations, namely material balances, scheduling and economic calculations (Figure 2A). First, operational inputs for each manufacturing process are ranked (GSA I), considering only batch size B, process time T, and cycle time Y as outputs. Inputs i which sum of first and second-order effects (S_T) results below a selected threshold of 0.05 are deemed to have a negligible contribution to output variability and excluded from the

reduced input sets. The first reduced set of operational inputs is combined with the full set of resource cost inputs (GSA II) to determine the most impactful inputs on throughput-related quantities. Additionally capital costs C, operating costs O and K are considered. A second reduced set of inputs is again obtained based on the selected threshold of significance and simulated via GSA III. All three levels of the staged three-step GSA are performed assuming uniform input distributions. This allows unbiased characterization of Sobol indices and observed sensitivities across the entire feasible range of the studied inputs. The knowledge acquired via this step provides an understanding of input–output sensitivities and assists the interpretation of the UA.

2.3.2 | Uncertainty analysis

Based on the outcomes of the GSA, the impact of uncertainty of critical inputs ($S_T \geq 0.05$) on the outputs is quantified. For this, techno-economic models at different scales are simulated iteratively for 4096 quasi-random input samples. In advanced manufacturing processes, the nature of uncertainty can differ, based on the level of process understanding acquired. To cater for all steps across process development and commercial scale, we propose the investigation of two types of uncertainties. The first one is the *epistemic* uncertainty, considering significant lack of process understanding and therefore uniform distributions for the inputs. In this case, we capture both the theoretical best and worst performance of the process. The second type of uncertainty is the *aleatoric* uncertainty, whereby process knowledge has been established and therefore the most likely input value can be identified. To assess such cases, we use triangular distributions based on reported upper and lower input bounds and a most probable value which corresponds to the nominal input considered for the techno-economic assessment.

3 | RESULTS AND DISCUSSION

3.1 | Techno-economic analysis of vector processes

Each of the developed flowsheets is simulated in Super-Pro with all inputs held at the base case values to determine nominal throughputs and costs of each manufacturing platform for process comparison. Capital costs attributed to seed cell expansion steps (1–3) (Figure 2A–C) are estimated to the same for the three processes and $\sim 40 \times 10^6$ \$ (Figure 3A–C). Although equipment dimensions and direct fixed cost correspond
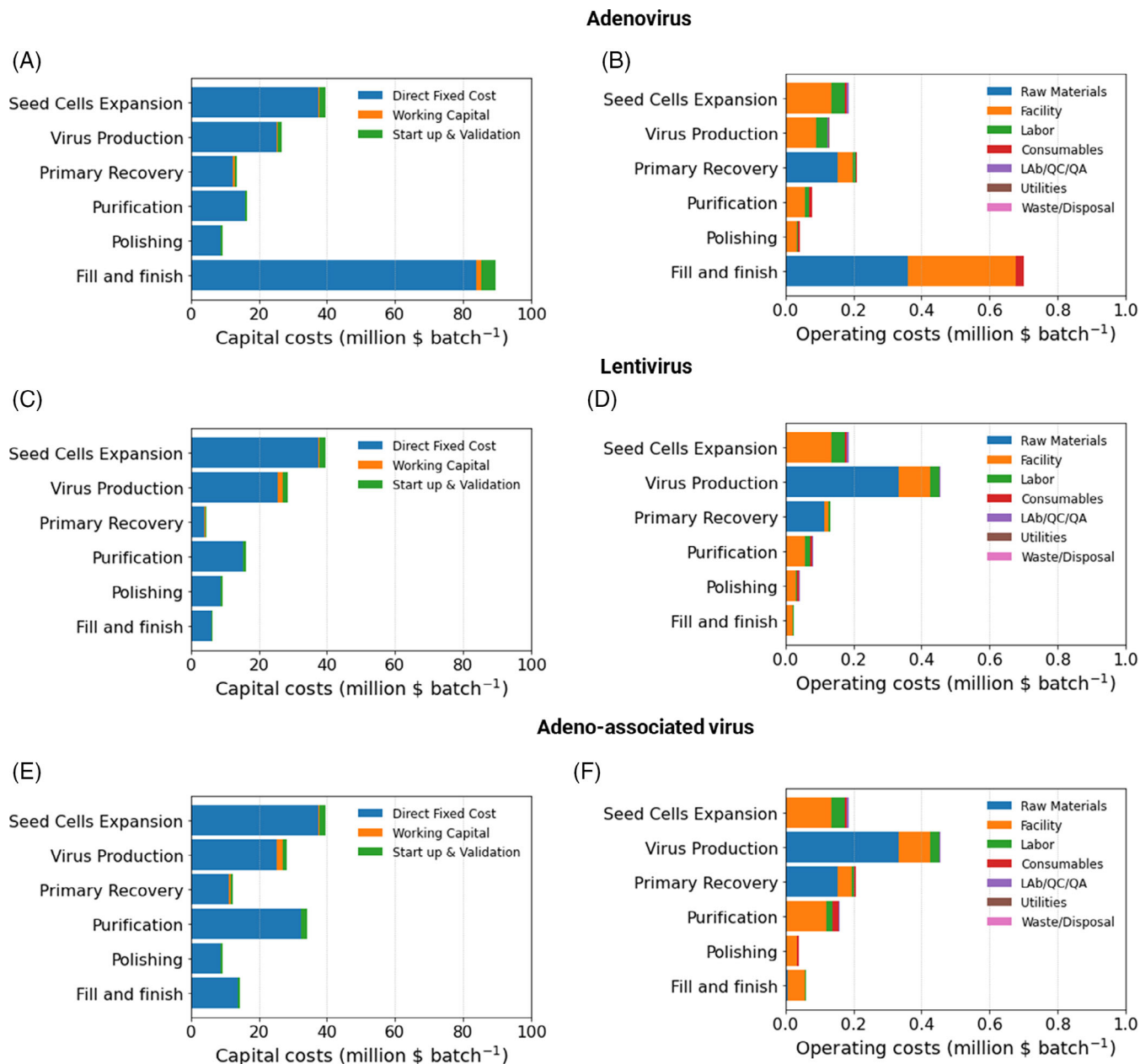
Adenovirus

Lentivirus

Adeno-associated virus

FIGURE 3 Breakdown of costs of manufacturing for viral vector processes: (A) capital costs for adenoviral (AdV), (B) operating costs for AdV, (C) capital costs for lentiviral (LV), (D) operating costs for LV, (E) capital costs for adeno-associated vector (AAV), (F) operating costs for AAV.

to 62×10^6 \$ for all processes in the virus production section as well, LV and AAV require an additional upfront working capital 1.6×10^6 \$ related to plasmid-based transfection. Upfront working capital covers for 30 days of operation (OpEx per month) and the raw materials in this section (plasmid DNA) make up ~77% of the OpEx per batch contribution for the virus propagation process section (Figure 3D,F).

The primary recovery and clarification steps require similar equipment purchase cost for AdV and AAV 11–12×10^6 \$, which result higher than equipment costs LV $(3 \times 10^6$ \$), as the supernatant can be harvested,

microfiltered and degraded without UF steps. As LV are extracellular entities and there is not an additional expenditure in lysis buffers, reduces the OpEx per batch brought by raw materials. In the case of AdV and AAV instead, lysis and Benzonase share 1.9×10^5 \$/batch of the OpEx per batch (Figure 3B,F).

The purification train for AdV and LV involves IEX and UF/DF steps. As expected, the AAV purification section involves an additional affinity chromatography step which comes with additional consumables costs (~6187\$/batch) and facility-dependent costs (~3.2×10^4 \$/batch) due to maintenance and equipment depreciation

(Figure 3A,F). As the number of cycles remains the same, a smaller bed volume is required and is proportional to the assumed volumetric flowrates and the column binding capacity. Capital costs in the polishing step result similar across all processes (8.6–8.8×10^6 $), as there are small deviations in the stream volumetric flowrates.

The F&F steps of the process entail different equipment sizes, because of the dilution targets in each vial. With a vial price at 2 $/vial, the AdV product is more diluted and is filled in smaller vials (5 mL). This results in a need for equipment at higher throughput (maximum 400 vials/min), in three parallel lines and many vials required. This translates into a substantial raw material costs (3.3×10^4 $/batch), as can be seen in Figure 3A. An additional cost contributor is the maintenance and depreciation cost, which directly depends on the capital cost. AAV and LV gene therapies require equipment of capacity <25 units/min, bypassing the need for parallel lines and requiring a smaller number of vials as products are more concentrated.

The time to produce a batch ranges around 22 days, with ∼95% of this contributed by the USP process and DSP time taking 20.5 days for each of the processes, respectively. As labor cost is estimated as a function of a basic labor rate and the hours of operation per batch, the labor cost contribution to OpEx per batch results the same for all processes as batch time is the same across all vectors. The bottleneck step in each of the process configurations is the cell culture step and viral growth in the main bioreactor and corresponds to ∼6 days, which becomes the shortest time between two consecutive batches within a manufacturing campaign. The maximum throughput of each facility results to be the same, namely 50 batches/year. This is computed by assuming a single year-long production campaign.

The batch sizes that result from each process are of significantly different orders of magnitude. The AdV process produces a nominal value of 3.0×10^6 doses/batch of AdV, compared to 214 LV doses/batch and 102 AAV doses/batch. The resulting nominal costs per dose are 0.5 $/dose for the AdV vaccine, 11 600 $/dose of the AAV *in vivo* gene and 1650 $/dose for LV products for *ex vivo* gene therapy. The results are found to agree with the orders of magnitudes for batch sizes and costs per dose reported in literature.[22–24,47,48]

3.2 | GSA and UA across platforms

The techno-economic analysis (Section 3.1) provides useful insights into the breakdown of costs and productivity drivers of each vector platforms at nominal point of operation at 2000 L scale. In this work, the equipment size is kept fixed and GSA is performed. GSA plots in Figures SI2-1–SI2-3A–C illustrate which key operational inputs propagate to the throughput quantities that define the productivity of the process (i.e., batch size, process time, and cycle time). The highest-ranked operational inputs are the used in combination with inputs for each resource cost (Figures SI2-1–SI2-3D–F) to screen a final set of critical operational and resource inputs, which are the basis of the following analyses.

3.2.1 | Throughput outputs

By considering the range of titers reported in the literature (Tables SI1-5–SI1-7) and recoveries for the DSP and F&F section, a range of batch sizes for each process is recorded. Given the dose sizes for the selected product applications and 2000 L scale of USP, AdV vaccines are produced at batch sizes at million dose scale, with ranges around 1.8×10^6 doses/batch (IQR = 1.1×10^6–2.9×10^6 doses/batch), several orders of magnitude higher than both AAV batches sizes, which distribute around a median of 76 doses/batch (IQR = 53–102 doses/batch) and LV, with a median of 672 doses/batch (IQR = 354–1133 doses/batch) (Figure 6A1–C1). First-order sensitivity indices S_i (Figure 4G–I) highlight that viral vector batch size variability is primarily caused by the titer input variability followed by the performance of the chromatography steps. Titers and working volumes vary within orders of magnitude up to $O(10^2)$ and are expected to result in larger variance in the batch size, as opposed to DSP recoveries which translate into a 0–1 fractional change of the batch size. This is seen in the AdV process, where the USP titer, working volume and IEX yield have respective first-order contributions S_i of 0.50, 0.35, and 0.06. Significant combined effects between titer and working volume are observed ($S_{ij} = 0.06$), as well as weaker interactions ($S_{ij} = 0.01$) with the IEX yield for both inputs. Similar trends are seen in the LV process, with first-order effects for the USP titer ($S_i = 0.53$), working volume ($S_i = 0.20$) and IEX yield ($S_i = 0.14$) on batch size variability. Combined effects between USP titer and working volumes ($S_{ij} = 0.03$) are observed alongside those with the IEX step ($S_{ij} = 0.01$). Finally in AAV manufacturing, first-order effects are once more observed for inputs related to USP productivity, namely USP titer ($S_i = 0.68$) and working volume ($S_i = 0.11$). The recovery of the affinity chromatography step stands out as impactful to batch size ($S_i = 0.05$), stronger than the IEX step ($S_i = 0.02$), which was in fact excluded at the GSA I step (Figure SI2-3). Despite sampling over an equivalent range of chromatography yields, the fractional change in the IEX is computed on a smaller batch size, which results in
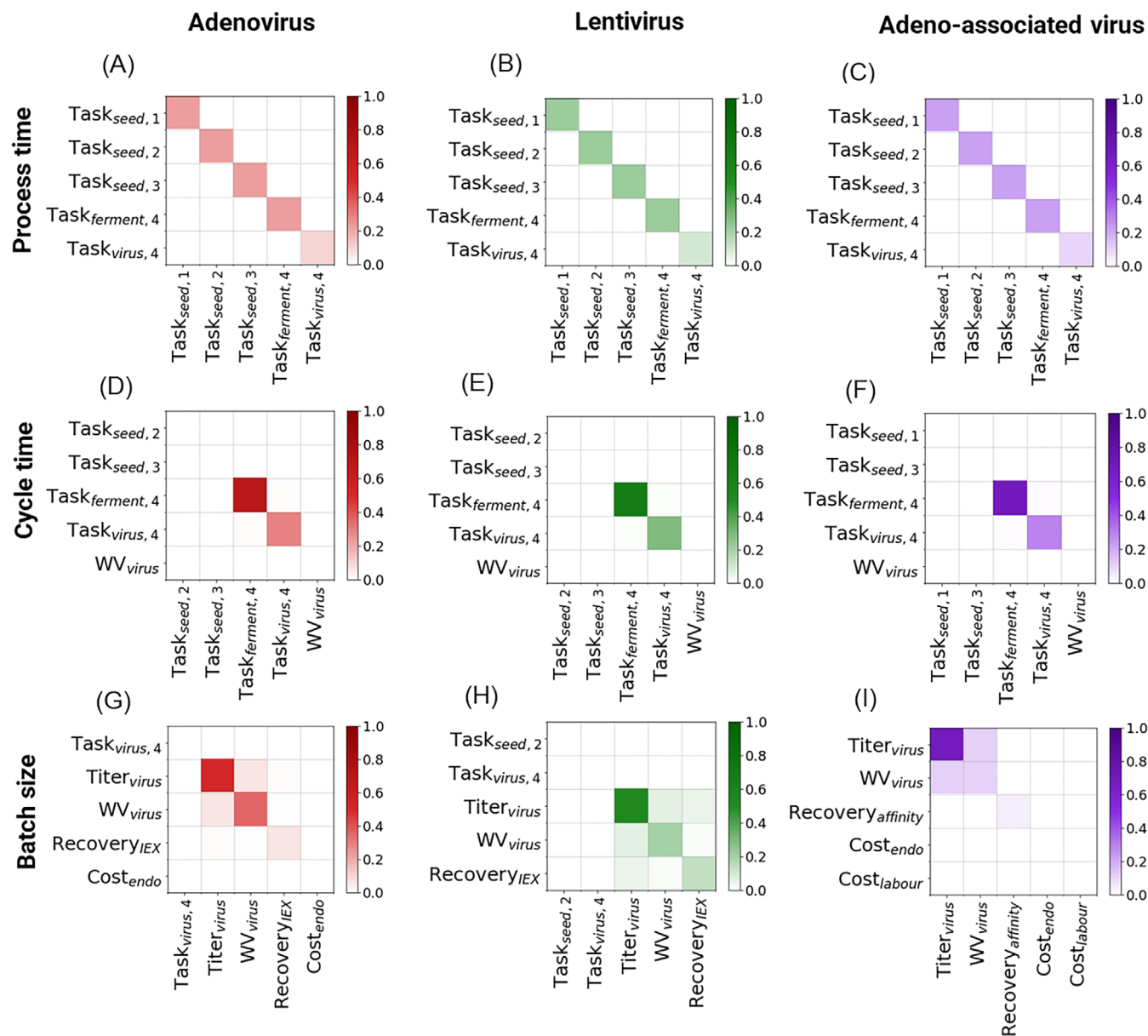
FIGURE 4 Global sensitivity analysis (GSA) plots for throughput-related outputs of each viral vector platforms. Each plot displays first-order sensitivity indices S_i along the diagonal and second-order indices S_{ij} in squares combining two inputs: (A) process time for adenoviral (AdV), (B) process time for lentiviral (LV), (C) process time for adeno-associated vector (AAV), (D) cycle time for AdV, (E) cycle time for LV, (F) cycle time for AAV, (G) batch size for AdV, (H) batch size for LV, (I) batch size for AAV. Only the five highest ranking inputs are included in the plot to aid visualization; full plots are displayed in Figures SI2-4–SI2-6.

lower contributions to the computed batch size variance. A strong combined effect on the output ($S_{ij} = 0.11$) is observed for USP titer and working volume, while interactions with chromatography yields remain lower ($S_{ij} < 0.05$). Filtration steps such as UF/DF do not impact the batch size significantly, with indices S_i do not go above 0.0001 (Figure SI2-2). These purification steps tend to be rather standardized in the industry, with recoveries that do not go below 90% for both AdV and AAV. In the case of LV instead, filtration recoveries can reach 70% as reported by Perry et al.[18] As a result the variability

introduced by titer and chromatography step yields is remarkably more significant.

The length of time to produce the batch solely depends on the assumed task lengths (Figure 4A–C). As processes are assumed to not be vector specific until transfection/infection and the longest tasks take place in the USP section, variability in process time is mainly attributed to task durations in the seed cell culture train (Steps 1–3) and the main bioreactor (Step 4), followed by viral growth. This is confirmed by the value of sensitivity indices ($S_i = 0.22$) for all cell tasks for all processes and

the viral vector growth with a lower index ($S_i = 0.099$). This results into a cycle time which ranges of 6.7 days (IQR = 6.1–7.5 days). The cycle time for each of the processes is impacted by the cell culture step duration in the main bioreactor ($S_i = 0.69$) and the transfection task length ($S_i = 0.28$) which together constitute the bottleneck of the process (Figure 4D–F).

3.2.2 | Cost outputs

A further set GSA plots is obtained, which illustrate how the combination of critical operational inputs and resource cost inputs impact cost-related outputs, including capital costs, operating costs per batch and operating cost per dose. The resulting uncertainty ranges are displayed in Figure 6A4–A6, B4–B6, and C4–C6.

Capital costs do not demonstrate significant variations across all platforms. This can be attributed to the fact that the equipment size is fixed and the largest share of this cost is the direct fixed cost. The recorded CapEx variability for all processes, with medians of 242.7×10^6 \$ (IQR = 242.4–243.0×10^6 \$) for AdV, of 128.5 (IQR = 127.9–129.0×10^6 \$) and of 170.2×10^6 \$ (IQR = 169.7–170.7×10^6 \$) for AAV is a result of varying working capital, which is estimated as a function of OpEx per year (Figure 5A–C). The working capital includes the upfront cost of materials for the initial 30 days of operation. This cost would be expected to vary according to the cost of the resources consumed for each batch and the actual number of batches completed within the 30-day period. Therefore, pDNA cost is the main contributor to working capital variability in the LV process ($S_i = 0.57$) and the AAV process (S_i of 0.47) followed by contributions from other resources ($S_i = 0.01$–0.09) (Figure 5B,C). Weaker first-order contributions from inputs that impact bottleneck lengths and number of batches is also observed, namely the task lengths relate to cell expansion and viral propagation in the main bioreactor ($S_i = 0.08$–0.19). In the case of AdV, first-order effects for these task lengths ($S_i = 0.52$, $S_i = 0.21$) prevail over materials resource costs (Figure 5A).

The variability in OpEx per batch for each vector is primarily introduced by materials and operating costs (Figure 5D–F). Given the inputs considered and the equipment size remaining fixed, the facility-dependent component of the cost does not contribute to the observed output variability. Plasmid DNA cost is the most prominent in LV ($S_i = 0.89$) and AAV manufacturing ($S_i = 0.75$) as it contributes to the largest share of the cost (Figure 5E,F) (Section 3.1, and References 22, 23, and 39). The OpEx per batch also varies due to the cost of endonuclease, with first-order contributions in both the

LV process ($S_i = 0.09$) and the AAV process ($S_i = 0.09$). A range of weaker first-order sensitivities ($S_i = [0.08$–$0.02]$) are also observed with respect to labor and medium cost in both LV and AAV manufacturing. GSA for the AdV process highlights stronger first-order effects for endonuclease costs ($S_i = 0.41$) and the labor rate ($S_i = 0.32$), as pDNA is not consumed by the process (Figure 5D). Additionally, the amount of medium consumed and its cost show significant first-order ($S_i = 0.14$) and weak second-order effects ($S_{ij} = 0.01$), as they impact the total cost of medium consumed which is factored in the materials cost. This second order effect becomes insignificant in LV and AAV manufacturing given the stronger S_i of pDNA cost. The computed uncertainty ranges for the OpEx per batch highlight that manufacturing a batch of AdV overall remains more expensive than LV and AAV vectors at the same scale (Figure 6A5–C5). Specifically, expenditures at medians of 1.41×10^6 \$/batch (IQR = 1.37–1.45×10^6 \$/batch) are required to manufacture AdV, due to the facility-dependent cost of the F&F sections. Manufacturing a batch of AAV vectors requires around 1.31×10^6 \$/batch (IQR = 1.22–1.39×10^6 \$/batch) as opposed to 0.98×10^6 \$/batch (IQR = 0.90–$1,07 \times 10^6$ \$/batch) for LV. This is because AAV costs embed additional expenditures for depreciation, materials, labor, and consumables of additional steps, for instance the affinity chromatography step.

With the range of OpEx per batch and batch sizes, a range of costs per dose for each product application is obtained (Figure 6A6–C6). AdV require smaller dose sizes, which improves the throughput of each batch and lowers the unit production cost to a median of 0.74 \$/dose (IQR = 0.48–1.16 \$/dose) (Figure 6A6). As batch sizes remain low for LV and AAV and dose sizes generally higher, the cost to produce a dose of LV product ranges within 1459 \$/dose (IQR = 866–2730 \$/dose) (Figure 6B6). Instead, AAV products cost ~17 268 \$/dose (IQR = 12 698–24 602 \$/dose) (Figure 6C6). The cost per dose is lowered for larger batch sizes and the GSA plots (Figure 5G–I) highlight how this value is mostly sensitive to the operational inputs that impact the batch size. In AdV manufacturing, first-order effects from USP titer ($S_i = 0.57$), working volume ($S_i = 0.30$) and IEX yield ($S_i = 0.042$) are recorded (Figure 5G). Similarly in LV manufacturing, significant inputs include USP titer ($S_i = 0.80$), working volume ($S_i = 0.60$) and IEX yield ($S_i = 0.036$) (Figure 5H). In AAV manufacturing, the impact of pDNA cost also results significant ($S_i = 0.09$), alongside the expected USP titer ($S_i = 0.41$), working volume ($S_i = 0.27$) and affinity chromatography yield ($S_i = 0.036$) (Figure 5I). This would be explained by the strong first-order contribution found for the OpEx per batch in AAV manufacturing, based on which the unit
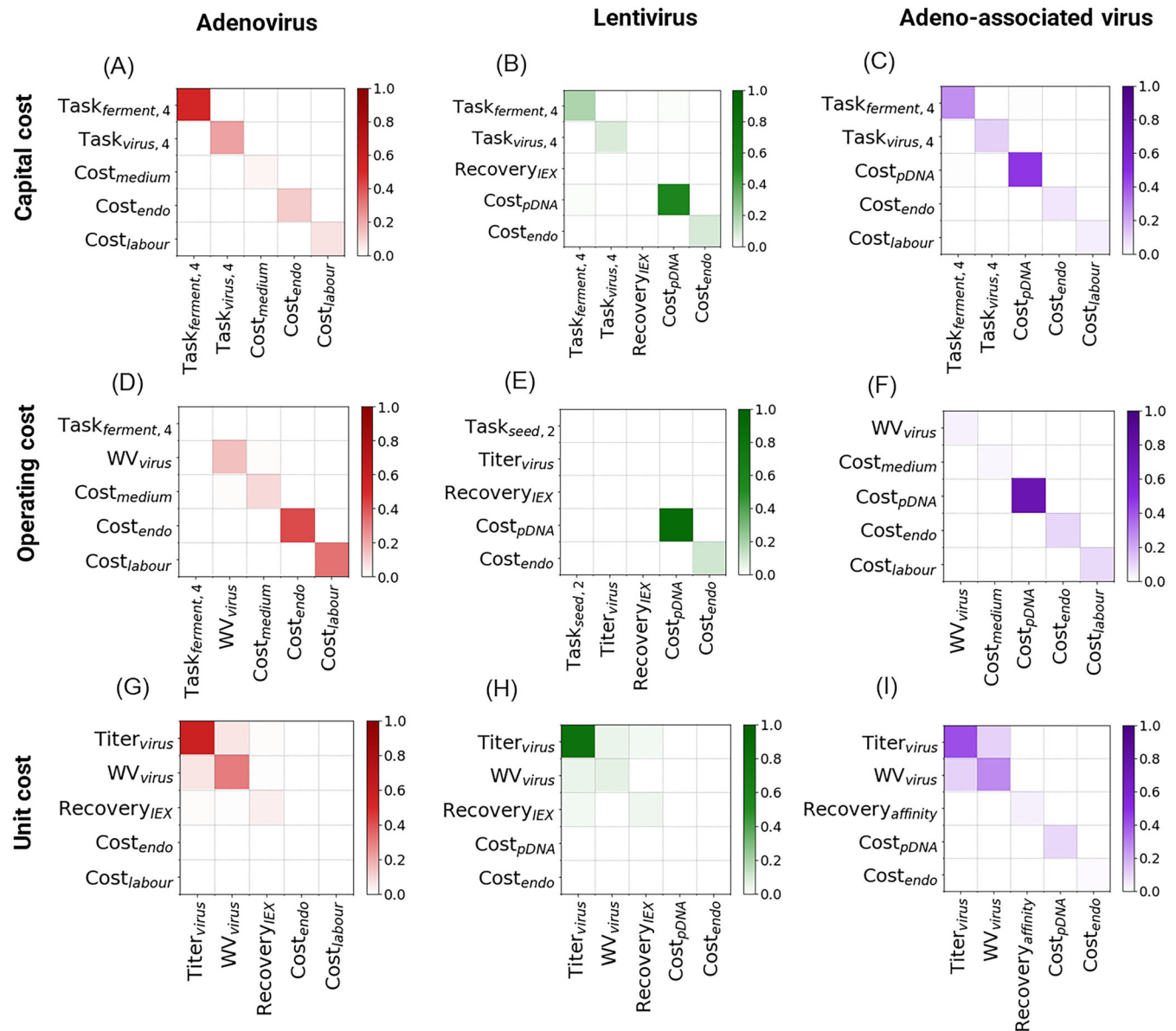
FIGURE 5 Global sensitivity analysis (GSA) plots for cost-related outputs of each viral vector platforms. Each plot displays first-order sensitivity indices S_i along the diagonal and second-order indices S_{ij} in squares combining two inputs: (A) Capital cost for adenoviral (AdV), (B) capital cost for lentiviral (LV), (C) capital cost for adeno-associated vector (AAV), (D) operating cost for AdV, (E) operating cost for LV, (F) operating cost for AAV, (G) unit cost for AdV, (H) unit cost for LV, (I) unit cost for AAV. The five highest ranking inputs are included in the plot to aid visualization; full plots are displayed in Figures SI2-4–SI2-6.

cost is computed. Second-order effects between USP titer, working volume and chromatography yields also propagate to the unit production cost, given its dependence on batch size. These results highlight the importance of either improving the productivity per batch and/or lowering dose sizes. It is in fact expected that lowering dose for gene therapy LV and AAV products especially would lower costs of production per unit by orders of magnitude. Additionally, reducing pDNA requirements for transfection would contribute to lowering AAV unit costs production. The orders of magnitude of costs and batch sizes are found to agree with data reported in literature and industrial reports.[22–24,27,47–49]

3.3 | Comparative analysis across platforms and scales

The GSA analyses (Section 3.2) and quantified Sobol indices provide useful insights how input uncertainty may propagate to process performance indicators for each viral vector platform considered. Leveraging on this
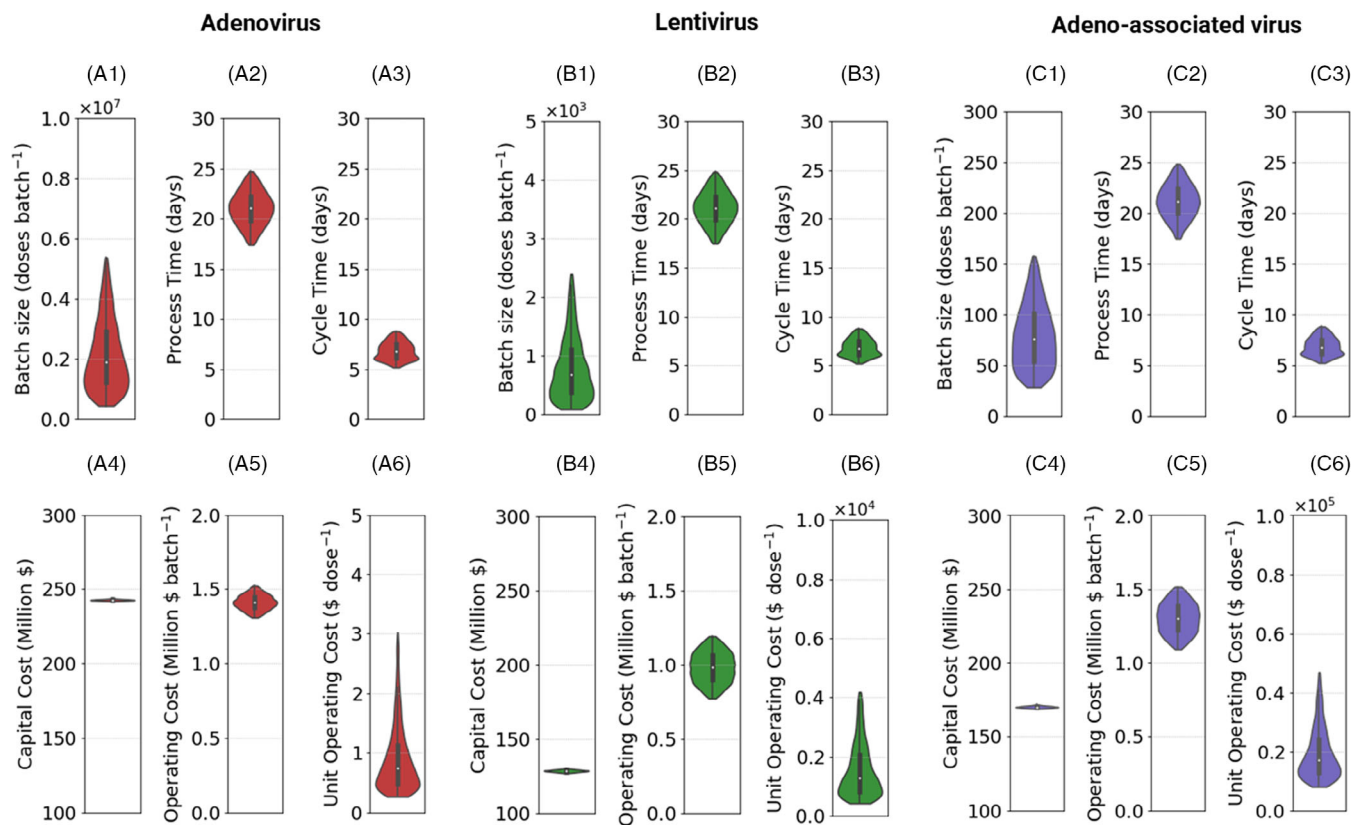
FIGURE 6 (A1–A6) Violin plots generated via uniform input distributions for adenoviral (AdV) process techno-economic performance, at 2000 L scale and assumed product dose size of 5×10^{10} VP dose-1: (A1–A3) throughput related outputs and (A4–A6) cost-related outputs. (B1–B6)—Violin plots for lentiviral (LV) process techno-economic performance, at 2000 L scale and assumed product dose size of 2×10^{9} TU dose-1: (B1–B3) throughput related outputs and (B4–B5) cost-related outputs. (C1–C6)—Violin plots for adeno-associated vector (AAV) process techno-economic performance, at 2000 L scale and assumed product dose size of 7×10^{14} vg dose-1. (C1–C3) throughput related outputs and (C4–C6) cost-related outputs.

knowledge, uncertainty ranges for each KPI at different scales of manufacturing can be quantified and characterized. First, a discussion on the propagation of uncertainty across scales is presented. Output uncertainty ranges generated via uniform sampling of the input space are compared with those generated via triangular distributions, to illustrate the impact of integrating process knowledge of most probable input values. Median and IQR ranges for each case are reported in Tables SI3-1–SI3-3 alongside violin plots for (i) process time, (ii) cycle time, (iii) capital cost, and (iv) operating cost per batch across scales (Figure SI3-1). Batch size ranges and cost per doses are instead presented in Figure 7. Secondly, a discussion on how scalability assessments can integrate the findings of the UA is presented.

3.3.1 | Throughput outputs

Process and cycle times ranges remain almost unchanged across scales (Figure SI3–A1–A2, B1–B2, C1–C2), and this is due to the assumption that the number of

expansion steps and task lengths do not vary across scales. When the uncertainty space is explored uniformly, medians of process times result around 21.2 days (IQR = 19.9–22.5 days) while a median cycle time of 6.8 days (IQR = 6.1–7.6 days) is found for all processes. When triangular distributions are assumed, more input samples are generated around the most probable value of 3.6 days for cell expansion tasks and 2 days for viral growth. Output samples result distributed around lower median values and a tighter IQR range is recorded, with medians of ~19.8 days (IQR = 18.9–20.8 days) for process time and 6.1 days (IQR = 5.8–6.9 days) for cycle time.

A volumetric propagation of uncertainty is observed with respect to the batch size for all production platforms and distributions, with larger IQR ranges as production scale increases (Figure 7A–C). This is due to the assumption that titer ranges do not vary across scales and directly multiply main bioreactor working volume which increases proportionally with scale. Additionally, the criticality of USP titer for batch size variability identified via GSA (Section 3.2) explains the prevalence of this trend
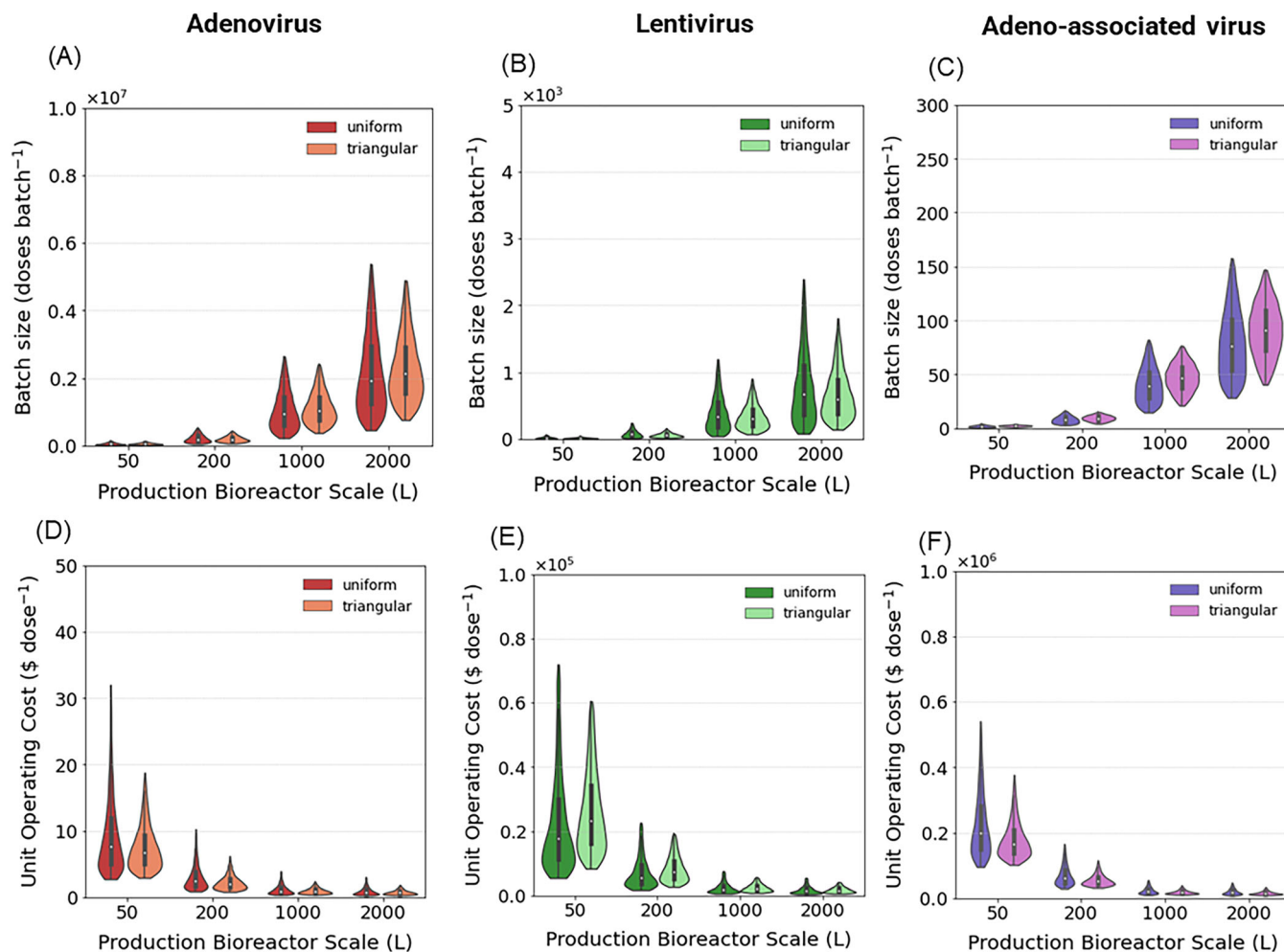
FIGURE 7 (A–D)—Violin plots for adenoviral (AdV) process techno-economic performance across scales (50–2000 L) and assumed product dose size of 5×10^{10} VP dose-1. (A) Batch size and (D) unit operating cost per dose. (B–E)—Violin plots for lentiviral (LV) process techno-economic performance across scales (50–2000 L) and assumed product dose size of 2×10^{9} TU dose-1. (B) Batch size and (E) unit operating cost per dose. (C–F)—Violin plots for adeno-associated vector (AAV) process techno-economic performance across scales (50–2000 L) and assumed product dose size of 7×10^{14} vg dose-1. (C) Batch size and (F) unit operating cost per dose. Uniform and triangular distributions are compared.

over the impact of DSP recoveries, which correspond to a fractional change in batch size and would contribute to a linear increase instead. Batch sizes for AdV-based vaccines applications consistently remain larger than LV-based and AAV-based gene therapies. Specifically, when considering a uniform distribution, AdV batch sizes range at 2000 L around medians of 1.9×10^{6} doses/batch (IQR = 1.2–2.9×10^{6} doses/batch), decreasing to a median of 9.4×10^{5} doses/batch (IQR = 5.9×10^{5}–1.4×10^{6} doses/batch) at 1000 L scale, up to a median of 4.7×10^{4} (IQR = 2.9×10^{4}–7.2×10^{4} doses/batch) at 50 L (Figure 7A). Compared to AdV, LV batch sizes remain lower ranging from around 672 doses/batch (IQR = 354–1133 doses/batch) at 2000 L to batch sizes of 17 doses (IQR = 9–28 doses/batch) at 50 L (Figure 7B). Median values for AAV batches at 2000 L correspond to

~76 doses/batch (IQR = 53–102 doses/batch) and drop to significantly lower amounts at 50 L, with 2 doses/batch (IQR = 1–3 doses/batch) (Figure 7C). If a triangular distribution is assumed, tighter ranges of batch sizes are observed for each scale, with the peak value selected for USP titers and recoveries impacting the shape of the distribution. In the LV process, most probable input values for USP titer and DSP recoveries are generated at a midpoint within the considered range and this translates in a symmetrically skewed distribution compared to the uniform case, with median values preserved for all scales and tighter IQR ranges. In the case of AdV and AAV, USP peak values correspond to the upper bound whereas IEX and affinity chromatography yields correspond to the lower bound. As USP titer is identified as most impactful to this output, median values for AdV and

AAV batch sizes increase for all scales while IQR ranges decrease, as more USP titer input samples are generated in the upper end of the specified ranges.

3.3.2 | Cost outputs

Smaller scales result in lower capital investments as equipment of smaller volume is required in each process. AdV capital costs drop from a median of 242.7×10^6 \$ (IQR $= 242.4$–243.0×10^6 \$) at 2000 L to 80.5×10^6 \$ (IQR $= 80.5$–80.6×10^6 \$) at 50 L scale (Figure SI3-1, A3). Overall, the process requires the highest capital expenditure compared to LV and AAV due to the F&F process sections at all scales. LV capital costs range from 128.5×10^6 \$ (IQR $= 128.2$–128.9×10^6 \$) at 2000 L to 71.3×10^6 \$ (IQR $= 71.2$–71.4×10^6 \$) at 50 L scale (Figure SI3-1,B3), whereas in AAV manufacturing at 50 L capital costs remain higher than LV, resulting in a median of 91.6×10^6 \$ (IQR $= 91.5$–91.7×10^6 \$) (Figure SI3-1,C3). Uncertainties around the capital costs remain narrow at all scales, with a variability introduced via the working capital contribution.

Scaling down batch sizes results in lower operating expenditures per batch for all vectors. Production costs for AdV batches remain higher than AAV batches and LV batches at all scales. For instance, in the uniform distribution case AdV production costs decrease from 1.41×10^6 \$/batch (IQR $= 1.37$–1.45×10^6 \$/batch) at 2000 L, to costs at 1000 L at medians of 0.90×10^6 \$/batch (IQR $= 0.87$–0.93×10^6 \$/batch) up to 0.36×10^6 \$/batch (IQR $= 0.33$–0.38×10^6 \$/batch) at 50 L (Figure SI3,A4). These ranges remain higher than the LV and AAV process scales, although processes converge to an almost equivalent expenditure of medians 0.32–0.39×10^6 \$/batch at 50 L (Figure SI3,B4,C4). Additionally, assuming triangularly distributed resource costs with central peak values results in a symmetrical tightening of IQR ranges around preserved median values. OpEx per batch is strongly dependent on resource costs realizations as observed in the GSA analyses and the distribution pattern is preserved. For both distributions larger IQR are observed with increasing scale due to the larger amount of raw material required to manufacture larger batch sizes.

Unit production costs result higher at lower scales due to economies of scale for all processes, with a 10–20-fold increase at 50 L compared to 2000 L (Figure 7D–F). If OpEx per batch for each vector is at similar orders of magnitude, converging to an equivalent range for smaller scale, differences across vectors are significant when costs are normalized by batch size ranges. Specifically, for the uniform distribution case, a 10-fold increase in unit cost for AdV-based vaccines translates in

an increase from 0.74 \$/dose (IQR $= 0.48$–1.16 \$/dose) at 2000 L to 7.56 \$/dose (IQR $= 4.90$–12.2 \$/dose) at 50 L (Figure 7D). For LV and AAV products, manufacturing at lower scale results in sharper increases in unit costs, as batch sizes are found to be lower by orders of magnitude compared to AdV vaccines. At 50 L scale, LV unit production costs range at 19127 \$/dose (IQR $= 11\,396$–36 640 \$/dose) compared to a median of 1459 \$/dose (IQR $= 866$–2730 \$/dose) at 2000 L scale (Figure 7E). Unit AAV costs at the lowest 50 L scale reach a median of 197 973 \$/dose (IQR $= 146\,360$–283 598 \$/dose) (Figure 7F). The impact of triangular distributions is also assessed and is related to the trends observed for the batch size for each vector application. These analyses highlight that manufacturing at larger scales is expected to lead to significant cost reductions, specifically in the case of ex vivo LV and in vivo AAV-based products which are characterized by smaller batch sizes and typically higher dose sizes.

3.3.3 | Scalability assessments and supply chain planning

A staged approach to scale up mitigates financial risks of investment, however, can reduce possible benefits from economies of scale in earlier phases of process development. In Phase I clinical trials, manufacturing is often allocated to existing small-scale assets. As clinical trials progress and product demand increases manufacturers may assess the maximum scalability of available resources before switching to larger scales. In this space, IQR ranges can be used as means of quantifying a worst-case and best-case performance for each KPI considered across scales. In addition, the shape of the probability distributions displays the likelihood of each scenario and can inform risk management strategies.

For instance, the UA conducted on the AAV process can be used to quantify the scalability of a 200 L production platform, which is estimated at ~11 doses/batch. This maximum value may be achieved via combined process improvements between USP processes via higher viral titers, operating bioreactors at maximized working volumes and improved affinity chromatography yields in DSP, which are found to be critical inputs for batch size variability. Unit production costs are directly impacted by batch size; therefore, in this best-case scenario would be lowered up to 44 886 \$/dose. Switching to larger scales a 1000 L bioreactor would ensure batch sizes of ~28 doses/batch at 28 900 \$/dose and ~53 doses at 14 874 \$/dose in the worst-case and best-case scenario respectively, with expected further cost reductions at 2000 L scale. For both

the uniform and triangular distribution case, the calculated IQR ranges are found to not overlap, which effectively improves confidence in the differentiation of process performance across scales. The high-dose requirements for AAV in vivo applications result in consistently lower batch sizes compared to other viral vector application. Prioritizing investments and process development efforts at higher scales in AAV manufacturing to maximize batch sizes would lead to substantial benefits from economies of scale. Manufacturers may assess the number of batches required at an intensified 200 L scale, compare it to the required number at larger scales and develop cost-effective strategies accordingly.

In the LV case, the quantified manufacturing uncertainties may result in more complex trade-offs during scale-up. Batch size outputs generated by uniform input distributions result in IQR ranges which overlap across scales as the spread of output samples increases, therefore challenging the differentiation of scales (Figure 7B). For instance, a 1000 L manufacturing process ensures batch sizes of around 336 doses/batch (IQR = 177–566 doses/batch) in the uniform distribution case. If production is allocated to this asset, manufacturers may compare the potential of process improvements (i.e., increasing viral titers and IEX yields) and assess switching to a higher scale. Figure 5B highlights a potential twofold increase in production in best-case process performance scenario, with a unit production cost of 1192 $/dose (Figure 5E). With scale up, a 2000 L process may supply batch sizes as low as 354 doses/batch in the worst-case scenario performance which corresponds to costs as high as 2 730 $/dose. The worst-case performance when more probable process parameters are integrated via triangular input distributions would instead correspond to 375 doses/batch at 2000 L and 2 578 $/dose. This highlights the importance of considering a drop in batch yields occurring during scale-up, as reversed effects to economies of scale may result from the scale switch. Nevertheless, when scenario probabilities are factored in the decision-making, switching to higher scales becomes a reliable option. Considering a hypothetical target demand of 500 doses and the batch size distributions obtained via uniform or triangular sampling, the 1000 L process displays a lower probability of satisfying it with a single batch in a best-case scenario compared to a 2000 L process at its worst-case performance, even prior to process intensification. In a similar fashion, the probabilistic cost per dose for each scale could be compared, as there is more probability of lowering unit production costs at 2000 L.

Further trade-offs emerge from an end-to-end supply chain perspective. Manufacturers supply the LV vectors as raw material for transfection for C&GT products ought to ensure raw materials availability at the cell therapy site, to allow minimized of return times of the end C&GT product to the starting patients. As more C&GT products reach commercialization and inventories of LV vectors are more likely to be depleted at the cell therapy manufacturing site, demand fluctuations may propagate to the LV supplier node as short-term unforeseen orders. This may pressure manufacturers in identifying proactive strategies to minimize collection times between batches, to ensure raw material availability for the manufacturing of life-saving C&GT therapeutics. In this space, the quantification of best- and worst-case cycle times of 5.9–7.4 days would assist manufacturers in assessing benefits of bypassing process bottlenecks in the main bioreactor through smaller scale equipment staggering. Shorter bottlenecks enable reactive short-term scheduling of new batches to fulfill short-term unforeseen orders. However, scaling out would however result in a reduced benefit from economies of scale, with associated probable batch sizes and costs and a requirement for a higher number of batches to meet established mid-term demand targets.

Scalability assessments in AdV-based vaccines applications highlights that a 1000 L manufacturing process provides batch sizes of around 9.4×10^5 doses/batch (IQR = 5.9×10^5–1.4×10^6 doses/batch), in the uniform distribution case (Figure 7D). Improved viral titers and IEX chromatography yields could enable ramping up production to 1.4×10^6 doses/batch at a cost 0.6 $/dose. In comparison, the worst-case performance of a 2000 L bioreactor correspond to 1.2×10^6 doses/batch, with costs of 1.16 $/dose. Further process improvements at this scale lowers cost to 0.5 $/dose, with >twofold increase in batch size, namely 2.9×10^6 doses/batch. Although these options result cost-competitive with unit costs ranging between 0.5 and 1.2 $/dose, the pressure to urgently supply vaccines at global scale may drive manufacturers to opt for investments at 2000 L. This would be because of a higher probability of larger batch sizes at million doses scale, which would meet global demand faster and provide a higher potential for scalability. Once more, considering the triangular distribution case, tighter IQR ranges would provide more confidence in the differentiation of performance of scales, as overlaps of uncertainties are reduced. From a supply chain perspective, the cost-competitiveness of AdV manufacturing at both 1000 and 2000 L scales, despite the considered uncertainties, highlights the potential of staggering equipment at a single location to reduce cycle time or decentralizing manufacturing assets across different geographical locations. Allocating resources in distributed supply chain networks allows manufacturing closer to the demand zones, minimize transport delays and costs and potentially improve the resilience of the network in case of

disruption, while potentially requiring a larger number of batches and longer production campaigns to meet demand targets.

4 | CONCLUSIONS

As more novel therapeutics advance from clinical to commercial stages, manufacturers are asked to plan their manufacturing capacity and schedule necessary equipment and facility investments such that shortage risks are minimized. This requires in-depth characterization of manufacturing platforms capabilities and incurred costs. The concept of *in risk* manufacturing is highlighting the need to plan before process capabilities are known for certain. In the case of viral vectors, processes still require significant improvements to maximize titers, minimize downstream (DSP) losses, shorten bottlenecks and reduce costs per dose. This holds especially for viral vector-based gene therapy products, where batch sizes are significantly higher than vaccines and costs result orders of magnitude higher. This study presents a systematic framework for (i) process modeling and simulation for the selected bio-pharmaceutical application for techno-economic assessment, (ii) characterizing of uncertainty in process performance, which involves correlating performance deviations to specific contributions of key process uncertainties (i.e., model inputs) via variance-based global sensitivity analysis (GSA), (iii) quantifying of uncertainty in the techno-economic performance (productivity and costs) (i.e., model outputs) at different scales of manufacturing. Our methodology is relevant to many other advanced therapy medicinal products (ATMP) emerging categories, such as mRNA vaccines and non-viral based gene therapies[50,51] and can repurposed for other product applications using the same vectors with adjusted dose sizes and adapting process models to alternative setups. In this work, processes for three vector applications are studied and compared, namely adenovirus-based (AdV) vaccines, lentivirus-based (LV) *ex vivo* gene therapy and adeno-associated virus-based (AAV) *in vivo* gene therapy.

Results of the techno-economic assessment for each platform suggest similar capital expenditures for the 2.000 L scale. Whereas operating expenditure for AdV embed a significant contribution from fill and finish (F&F) costs, a significant portion of LV and AAV production costs per batch corresponds to plasmid DNA requirements for viral propagation. As USP titers are typically higher, batch sizes for AdV are orders of magnitude larger than LV and AAV. As a result, costs of vaccines typically range around 0.5–1 $/dose, whereas gene therapies cost 1000–10 000$/dose in best-case scenarios.

GSA results highlight pressure points in viral vector manufacturing and set strategic targets for process improvements and engineering efforts. Sobol indices highlight how input uncertainty may propagate to process performance uncertainty. Batch sizes are found to be impacted mostly by upstream (USP) titers and working volumes, followed by DSP chromatography recoveries. Process bottlenecks for each of the processes are also characterized. As the process set up considered a single production line, cycle time is dictated by the tasks of cell and viral growth in the main bioreactor. Unit production cost per dose are found to be directly correlated to the batch size.

A comparative uncertainty analysis (UA) across scales is then presented and is aimed at quantifying uncertainty ranges for the selected throughput and cost related key performance indicators (KPIs) for different scales and vector products. Additionally, the impact of the assumed input probability distributions on KPI uncertainty is assessed, with comparisons between uniform and triangular input distributions. As triangular distributions result in tighter uncertainty ranges for all outputs considered, this is found to improve the differentiation of process performance across scales, which reduces risks associated with scale selection.

Despite uncertainties, investment in higher scales in early stages leads to significant cost reductions, specifically in case of AAV-based in vivo gene therapies, which are characterized by consistently smaller batch sizes. Scale-up assessments for LV manufacturing are also presented, with direct considerations related to risk quantification in switching to larger scales and meet set demand targets. Scale comparisons for AdV manufacturing platforms, highlight the cost-competitiveness of scaling out manufacturing resources at smaller scales and focusing on process intensification.

The analyses presented highlight several challenges related to minimizing production and distribution costs, while ensuring product availability and setting up flexible manufacturing platforms. Process performance uncertainty at different scales adds further risks for each scale up and investment decision. The framework presented in this study provides means of characterizing process performance ranges and associated probability distributions which ought to be integrated in the decision-making. This highlights the need for computer-aided tools that systematically integrate the scale dependent process uncertainties, quantify performance and risks of manufacturing alternatives. This would assist decision-makers in identifying successful strategies forward that ensure availability of ground-breaking therapeutics to those in need, from clinical to commercial stages.

AUTHOR CONTRIBUTIONS

Miriam Sarkis: Formal analysis (lead); investigation (lead); methodology (lead); validation (lead); visualization (lead); writing – original draft (lead). **Nilay Shah:** Supervision (equal); writing – review and editing (equal). **Maria Papathanasiou:** Conceptualization (lead); supervision (equal); writing – review and editing (equal).

CONFLICT OF INTEREST STATEMENT

The authors declare no conflicts of interest. [Correction added on 21 June 2023, after first online publication: COI statement added]

DATA AVAILABILITY STATEMENT

The data that support the findings of this study are available from the corresponding author upon reasonable request.

ORCID

Maria M. Papathanasiou https://orcid.org/0000-0002-8886-0624

REFERENCES

[1] EMA. Advanced therapy medicinal products: Overview. https://www.ema.europa.eu/en/human-regulatory/overview/advanced-therapy-medicinal-products-overview (accessed: June 2021).

[2] J. T. Bulcha, Y. Wang, H. Ma, P. W. L. Tai, G. Gao, *Signal Transduct. Target. Ther.* **2021**, *6*(53), 1.

[3] U.S. Food & Drug Administration. Approved Cellular and Gene Therapy Products.

[4] Cytiva. Strategies to address the viral vector manufacturing shortage. https://www.cytivalifesciences.com/en/us/solutions/bioprocessing/knowledge-center/strategies-for-viral-vector-manufacturing (accessed: June 2021).

[5] CHMP. Package Insert—LUXTURNA (Voretigene Neparvovec-Rzyl) **2018**. www.fda.gov/medwatch

[6] CHMP. Package Insert: ZONGELSMA (onasemnogene abeparvovec-xioi) **2019**. www.fda.gov/medwatch

[7] CHMP. Package Insert: KYMRIAH (tisagenlecleucel) **2019**.

[8] U.S. Food & Drug Administration (FDA). FDA approves CAR-T cell therapy to trat adults with certain types of large B-cell lymphoma. https://www.fda.gov/news-events/press-announcements/fda-approves-car-t-cell-therapy-treat-adults-certain-types-large-b-cell-lymphoma (accessed: March 2021).

[9] K. Lundstrom, *Viruses* **2021**, *13*(2), 317. https://doi.org/10.3390/v13020317

[10] R. Arthur, *Meeting demand: 3 ways to boost viral vector production.* **2021**. https://www.genengnews.com/topics/bioprocessing/advanced-therapies-could-be-sleepwalking-into-a-manufacturing-cost-crisis/ (accessed: February, 2023).

[11] E. Lambrix, H. Kent-Egan, *Biotech Rev. Year* **2021**, (9), 22.

[12] V. Raper, *Advanced therapies could be sleep walking into a manufacturing cost crisis* **2023**. https://www.genengnews.com/topics/bioprocessing/advanced-therapies-could-be-sleepwalking-into-a-manufacturing-cost-crisis/ (accessed: February, 2023).

[13] Novasep. Finding the good in everyone. https://www.novasep.com/media/novasep-viral-vectors-manufacturing-brochure-2019.pdf (accessed: June 2021).

[14] MilliporeSigma. Flexible manufacturing of vaccines. https://vertassets.blob.core.windows.net/download/36eec989/36eec989-3bf0-49a4-8f41-43f403dc6d87/ms_br5360en_flex_manufacturing.pdf (accessed: June 2021).

[15] Cytiva, *Optimization of Midstream Cell Lysis and Virus Filtration Steps in an Adenovirus Purification Process* **2020**. https://cdn.cytivalifesciences.com/api/public/content/digi-26781-pdf (accessed: November, 2022).

[16] ThermoFisher. Adherent Cell Culture vs. Suspension Cell Culture. https://www.thermofisher.com/it/en/home/references/gibco-cell-culture-basics/cell-lines/adherent-vs-suspension-culture.html (accessed: June 2021).

[17] E. Capra, A. Gennari, A. Loche, C. Temps, *Viral-Vector Therapies at Scale: Today's Challenges and Future Opportunities*, McKinsey & Company. **2022**, https://www.mckinsey.com/industries/life-sciences/our-insights/viral-vector-therapies-at-scale-todays-challenges-and-future-opportunities (accessed: November, 2022).

[18] C. Perry, A. C. M. E. Rayat, *Viruses.* **2021**, *13*(2), 268.

[19] O. W. Merten, M. Schweizer, P. Chahal, A. Kamen, *Pharm. Bioprocess.* **2014**, *2*(3), 237.

[20] O. W. Merten, M. Schweizer, P. Chahal, A. A. Kamen, *Pharm. Bioprocess.* **2014**, *2*(2), 183.

[21] O. W. Merten, S. Charrier, N. Laroudie, S. Fauchille, C. Dugué, C. Jenny, M. Audit, M. A. Zanta-Boussif, H. Chautard, M. Radrizzani, G. Vallanti, L. Naldini, P. Noguiez-Hellin, A. Galy, *Hum. Gene Ther.* **2011**, *22*(3), 343.

[22] R. M. Comisel, B. Kara, F. H. Fiesser, S. S. Farid, *Biochem. Eng. J.* **2021**, *167*, 107868.

[23] R. M. Comisel, B. Kara, F. H. Fiesser, S. S. Farid, *Biochem. Eng. J.* **2021**, *176*, 176.

[24] R. G. Ferreira, N. F. Gordon, R. Stock, D. Petrides, *Processes* **2021**, *9*(8), 1430. https://doi.org/10.3390/pr9081430

[25] Intelligen. SuperPro Designer (v12).

[26] Z. Kis, M. Papathanasiou, R. Calvo-Serrano, C. Kontoravdi, N. Shah, *J. Adv. Manuf. Process.* **2019**, *1*(3), e10025. https://doi.org/10.1002/amp2.10025

[27] Z. Kis, K. Tak, D. Ibrahim, M. M. Papathanasiou, B. Chachuat, N. Shah, C. Kontoravdi, *NPJ Vaccines.* **2022**, *7*(1), 29.

[28] N. E. Altaras, J. G. Aunins, R. K. Evans, A. Kamen, J. O. Konz, J. J. Wolf, *Adv. Biochem. Eng./Biotechnol.* **2005**, *99*, 193.

[29] L. Xie, W. Pilbrough, C. Metallo, T. Zhong, L. Pikus, J. Leung, J. G. Aunins, W. Zhou, *Biotechnol. Bioeng.* **2002**, *80*(5), 569.

[30] G. Jagschies, J. Joseph, E. Eriksson, in *Biopharmaceutical Processing: Development, Design and Implementation of Manufacturing Processes* (Eds: G. Jaschies, E. Lindskog, K. Lacki, P. Galliher), Elsevier, Amsterdam, The Netherlands **2018**, p. 637.

[31] S. Ansorge, S. Lanthier, J. Transfiguracion, Y. Durocher, O. Henry, A. Kamen, *J. Gene Med.* **2009**, *11*(10), 868.

[32] M. Bauler, J. K. Roberts, C. C. Wu, B. Fan, F. Ferrara, B. H. Yip, S. Diao, Y. I. Kim, J. Moore, S. Zhou, M. M. Wielgosz, B. Ryu, R. E. Throm, *Mol. Ther. Methods Clin. Dev.* **2020**, *17*, 58.

[33] A. P. Manceur, H. Kim, V. Misic, N. Andreev, J. Dorion-Thibaudeau, S. Lanthier, A. Bernier, S. Tremblay, A. M. Gélinas, S. Broussau, R. Gilbert, S. Ansorge, *Hum. Gene Ther. Methods* **2017**, *28*(6), 330.

[34] B. A. Thorne, R. K. Takeya, R. W. Peluso, *Hum. Gene Ther.* **2009**, *20*, 707.

[35] S. Cecchini, T. Virag, R. M. Kotin, *Hum. Gene Ther.* **2011**, *22*(8), 1021.

[36] J. C. Grieger, S. M. Soltys, R. J. Samulski, *Mol. Ther.* **2016**, *24*(2), 287.

[37] J. Konz, A. Lee, A. Goerke, C. S. B. To. *US20080118970A1*, 2007.

[38] S. Fedosyuk, T. Merritt, M. P. Peralta-Alvarez, S. J. Morris, A. Lam, N. Laroudie, A. Kangokar, D. Wright, G. M. Warimwe, P. Angell-Manning, A. J. Ritchie, S. C. Gilbert, A. Xenopoulos, A. Boumlic, A. D. Douglas, *Vaccine* **2019**, *37*(47), 6951.

[39] S. Petitt, C. Glover, J. Madsen, J. Pratik. *Key Considerations in Gene Therapy Manufacturing for Commercialization* **2018**.

[40] O. Terova, S. Soltys, P. Hermans, J. de Rooij, F. Detmers, *Cell Gene Ther. Insights.* **2018**, *4*(2), 101.

[41] J. de Rooij, J. de DeConto, G. Schaenzler, D. Bauer, K. Barre, M. Duskin, A. Kohli, K. Watanabe, *Cell Gene Ther. Insights.* **2019**, *5*(S5), 1017.

[42] W. Qu, M. Wang, Y. Wu, R. Xu, *Curr. Pharm. Biotechnol.* **2015**, *16*, 684.

[43] CHMP. Package Insert: Jansenn COVID-19 Vaccine **2021**. https://www.cdc.gov/vaccines/covid-19/clinical-considerations/managing-anaphylaxis.html

[44] CHMP. Package Insert: COVID-19 Vaccine AstraZeneca, COVID 19 Vaccine (ChAdOx1 S [recombinant]).

[45] CRB Group. The current state of aseptic processing & fill-finish manufacturing.

[46] A. Alshahibi, S. Gonzales, R. Yavuzt, T. Öner, E. Denizci, *Development of Sustainable Bioprocesses: Modeling and Assessment* (Eds: E. Heinzle, A. Biwer, C. Cooney, E. Denizci), John Wiley & Sons, Ltd., Chichester **2006**.

[47] P. Jones. presented at amc 19th Technical Meeting: Manufacturing ATMPs, Scale Dublin **2019**.

[48] E. Cameau, A. Pedregal, C. Glover, *Cell Gene Ther. Insights* **2019**, *5*(11), 1663.

[49] Z. Kis, C. Kontoravdi, A. K. Dey, R. Shattock, N. Shah, *J. Adv. Manuf. Process.* **2020**, *2*(3), e10060.

[50] M. Ramamoorth, A. Narvekar, *J. Clin. Diagn. Res.* **2015**, *9*(1), GE01.

[51] J. Whitley, C. Zwolinski, C. Denis, M. Maughan, L. Hayles, D. Clarke, M. Snare, H. Liao, S. Chiou, T. Marmura, H. Zoeller, B. Hudson, J. Peart, M. Johnson, A. Karlsson, Y. Wang, C. Nagle, C. Harris, D. Tonkin, S. Fraser, L. Capiz, C. L. Zeno, Y. Meli, D. Martik, D. A. Ozaki, A. Caparoni, J. E. Dickens, D. Weissman, K. O. Saunders, B. F. Haynes, G. D. Sempowski, T. N. Denny, M. R. Johnson, *Transl. Res.* **2022**, *242*, 38.

SUPPORTING INFORMATION

Additional supporting information can be found online in the Supporting Information section at the end of this article.

How to cite this article: M. Sarkis, N. Shah, M. M. Papathanasiou, *J. Adv. Manuf. Process.* **2023**, *5*(3), e10158. https://doi.org/10.1002/amp2.10158